PERGAMON

International Journal of Solids and Structures 36 (1999) 3591–3615

INTERNATIONAL JOURNAL OF SOLIDS and STRUCTURES

Mechanical behaviour of brittle matrix composites: a homogenization approach

Alberto Taliercio[a,*], Roberto Coruzzi[b]

[a] *Department of Structural Engineering, Politecnico di Milano, Piazza Leonardo da Vinci 32, 20133 Milan, Italy*
[b] *Department of Civil Engineering, University of Parma, 43100 Parma, Italy*

Received 21 May 1997; in revised form 5 May 1998

Abstract

A numerical model is developed with the aim of describing the macroscopic mechanical response of unidirectional brittle–matrix fiber-reinforced composites subjected to stresses acting in any plane transverse to the fibers. Finite element analyses of a representative unit cell are performed, with suitable boundary conditions ensuring continuity of the displacement field across adjacent cells and periodicity of the strain field over the cell. A strain–softening constitutive law is adopted for the matrix in tension to allow, for instance, for brittleness induced by possible defects in a polymeric matrix. The perfectly plastic case is also considered for sake of comparison. Results established for ductile composites are found to be inappropriate for brittle matrix composites: numerical analyses show that composites with softening matrix have transverse strength properties much poorer than perfectly plastic composites with matrix of equal strength, and even than the unreinforced matrix. An induced transverse anisotropy in the post-peak regime is also observed. A discussion on the proposed approach concludes the note.

1. Introduction

Micromechanics is widely employed to relate the overall properties of strongly heterogeneous media with the properties of the constituents and the microstructure. In this context, the term 'homogenization' usually qualifies the passage from the micro- to the macro-scale. The fundamentals of the methods mostly employed to evaluate, either exactly or approximately, a number of mechanical parameters for heterogeneous media of different nature are described by Suquet (1987), Aboudi (1991), Nemat-Nasser and Hori (1993), only to quote a few. A micromechanical approach gives useful insight into the mechanisms that control the global response of the material. Also, micromechanics allows in principle the design of new composites that have to fulfill certain behavioural constraints, by properly selecting the constituents and the geometry of the phases.

* Corresponding author. Fax: 0039 02 23 99 42 20. E-mail: talierci@rachele.stru.polimi.it

0020–7683/99/$ - see front matter
PII: S0020–7683(98)00167–X

Most works on homogenization address the elastic field that, historically, was the first to be explored. On account of the widespread use of metal–matrix composites, an important number of papers has been more recently published regarding the description of the macroscopic behaviour of elastic–perfectly plastic (Dvorak and Bahei-el-Din, 1987; Pindera and Aboudi, 1988) and strain-hardening (Aboudi, 1988; Dvorak et al., 1988; Dvorak and Bahei-el-Din, 1991) fiber-reinforced composites (FRCs). Techniques based on homogenization coupled with limit analysis provide estimates for the macroscopic strength of composites, either with perfect or imperfect interfacial bonding (de Buhan and Taliercio, 1991; Taliercio, 1992; Taliercio and Sagramoso, 1995). These results are of interest when only the overall bearing capacity of the composite is investigated and the entire macroscopic nonlinear stress–strain law is a detailed but unnecessary information. Micromechanical techniques have also been employed with reference to other types of material behaviour: the viscoelastic case has been studied since the pioneering works of Hashin (1965, 1966), based on the modelisation of a FRC as an assemblage of composite cylinders. Recently, sophisticated analysis methods have been formulated with reference to viscoplastic composites (Fotiu and Nemat-Nasser, 1996).

Beyond the elastic range, polymer–matrix composites are often assimilated to perfectly plastic materials—when the short-term response of these materials is analyzed and time effects can be neglected. Actually, thermosetting resins embedding flaws, possibly originated by the manufacturing process, exhibit a brittle behaviour in tension (Hull, 1981). Another important class of brittle–matrix composites, or BMCs, is obviously formed by ceramic composites. The number of works covering micromechanics applied to BMCs is rather limited: some of the works recently published on this subject are quoted hereafter. Bosco and Carpinteri (1995) investigated the flexural response of structural elements made of BMCs using a bridged-crack model. Dharani and Ji (1996) determined the local displacement field in a composite where a non-axisymmetric crack cuts part of the matrix. Hild et al. (1996) employed continuum damage mechanics to derive the macroscopic stress–strain law for a damaged composite: matrix cracking and interface debonding are described through microscopic damage variables. Zhang et al. (1996) focused their attention upon the evaluation of stress intensity factors associated with cracks in the matrix and at the fiber–matrix interface, assuming the uncracked matrix to be linear elastic. The quoted papers are mainly addressed to fiber composites loaded parallel to the fibers. Dealing with this specific loading condition allowed the authors of some of these papers to obtain solutions in a semi-analytical form. To the authors' knowledge, heterogeneous periodic media with brittle constituents have not been analyzed yet under general loading conditions.

This paper describes a numerical model to analyze unidirectional, long-fiber composites with strain–softening matrix, subjected to stresses acting in any plane transverse to the fibers. It is in this plane that matrix brittleness is likely to play the most important role, since the strengthening effect of the fibers is quite negligible. After having briefly recalled some elements of homogenization for periodic media (Section 2), the employed numerical model is illustrated in Section 3. First, the finite element discretization used to analyze a representative unit cell is described (Section 3.1); the kinematic boundary conditions that ensure periodicity of the microscopic strain field and continuity of the displacement field across adjacent cells are explicitly derived in an Appendix. The displacement boundary conditions that allow the simulation of elementary macroscopic strains and stresses over the cell are outlined in Section 3.2. The constitutive model adopted for the matrix material is described in Section 3.3: it is featured by a plastic strain–hardening response in

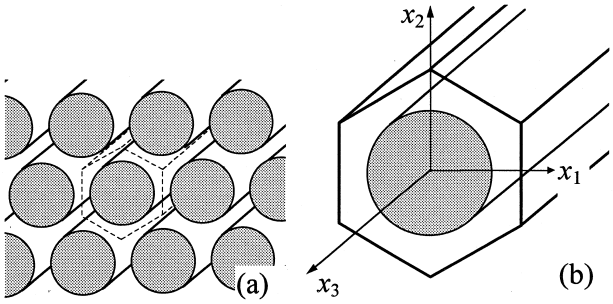

Fig. 1. (a) Unidirectional composite with hexagonal reinforcing array and (b) possible choice for the unit cell.

compression and a strain-softening behaviour in tension. Two post-peak softening responses are considered, one describing a gradual strength decay with strain and the other one featured by an abrupt drop in strength: the latter case is meant to be a first attempt to analyze ceramic composites, exhibiting perfectly brittle behaviour. Section 4 is devoted to numerical applications. The reliability of the numerical model in the elastic range is first checked in Section 4.1 through comparisons with experimental results. Then the results of analyses of the unit cell subjected to elementary transverse macroscopic stresses (e.g. uniaxial tension or pure shear) are illustrated and critically examined in Section 4.2; the perfectly plastic case is also considered for sake of comparison. A discussion about the sensitivity of the results to mesh refinement is made in Section 4.2.1. Merits and limitations of the proposed approach are discussed in a final section, where possible improvements and future developments are also outlined.

2. Homogenization theory: basic concepts

In dealing with highly heterogeneous media, it is customary to substitute the real medium with an ideal, homogeneous continuum with properties to be derived through analyses of a 'Representative Volume Element' (RVE—see e.g. Nemat-Nasser and Hori, 1993); the volume of the RVE will be indicated by V. Here, attention is focused on composite materials evenly reinforced by long, parallel fibers of equal section. If any randomness in the reinforcing array is neglected, unidirectional FRCs can be considered as periodic media. For this class of heterogeneous media, a single 'unit cell' can be taken as RVE. The entire periodic medium can be seen as a collection of contiguous, equal unit cells. Figure 1 shows a possible choice of unit cell for unidirectional composites with hexagonal reinforcing array: this is the case that will be considered in numerical analyses for its importance in applications. Indeed, with fibers of equal circular cross-section, a regular hexagonal array gives the highest percentage of reinforcement, which can ideally attain 91% of the total volume of the composite element. Note that the length of the unit cell along the fiber axis, x_3, is immaterial.

Stresses and strains at any point of the homogenized medium (also called 'macroscopic' stresses and strains and denoted by $\underline{\underline{\Sigma}}$ and $\underline{\underline{E}}$, respectively) are assumed to be the averages over any RVE of the corresponding local (or microscopic) quantities, $\underline{\underline{\sigma}}$ and $\underline{\underline{\varepsilon}}$. It is expedient to compute $\underline{\underline{\Sigma}}$ and

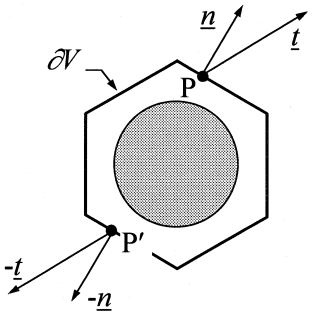

Fig. 2. Boundary tractions $\underline{t}$ taking equal and opposite values at two corresponding points, P and P′, of the boundary of any unit cell.

$\underline{\underline{E}}$ in terms of stresses and displacements along the boundary ∂V of the RVE (see e.g. Nemat-Nasser and Hori, 1993):

$$\underline{\underline{\Sigma}} = \frac{1}{|V|}\int_{\partial V} \underline{x} \otimes \underline{t}\, \mathrm{d}S; \tag{1a}$$

$$\underline{\underline{E}} = \frac{1}{|V|}\int_{\partial V} \frac{1}{2}(\underline{u} \otimes \underline{n} + \underline{n} \otimes \underline{u})\, \mathrm{d}S. \tag{1b}$$

Here, $\underline{x}$ denotes any point of the RVE and its boundary, $\underline{u}$ the microscopic displacement field, $\underline{n}$ the outward unit normal to ∂V and $\underline{t} = \underline{\underline{\sigma}} \cdot \underline{n}$ the boundary tractions. The symbol $\otimes$ denotes dyadic tensor product. Equation (1a) applies if body forces are neglected; incidentally note that, if $\underline{\underline{\sigma}}$ is divergence-free, the symmetry of $\underline{\underline{\Sigma}}$ is implicit in definition (1a). In applications, eqns (1a, b) allow a simplified computation of the macroscopic variables, in comparison with volume integrals over the RVE. Another advantage from using eqns (1a, b) is that these definitions apply also if the real medium embeds cracks, across which displacements are discontinuous, or pressure-free cavities. In these cases, ∂V must not intersect any void and must be intended as the outer boundary of the RVE (thus excluding the boundary of cracks and cavities).

In the case of periodic media, the microscopic fields have to fulfill suitable periodicity conditions ensuring continuity of boundary tractions and displacements across adjacent cells (see e.g. Suquet, 1987). $\underline{t}$ must take equal and opposite values at two corresponding points of ∂V (Fig. 2), i.e., $\underline{t}$ must be anti-periodic on ∂V, and $\underline{u}$ must be of the form

$$\underline{u}(\underline{x}) = \underline{\underline{E}} \cdot \underline{x} + \underline{v}(\underline{x}) \tag{2}$$

with $\underline{v}(\underline{x})$ periodic over V. A displacement field fulfilling eqn (2) is also said to be 'strain-periodic' (Suquet, 1987). No macroscopic strain is associated with $\underline{v}$. For periodic media, the appropriateness of $\underline{\underline{\Sigma}}$ and $\underline{\underline{E}}$ as mechanically meaningful macroscopic variables is furtherly supported by the rate-of-work equivalence (also known as 'Hill's macro-homogeneity equality'):

$$\underline{\underline{\Sigma}} : \dot{\underline{\underline{E}}} = \frac{1}{|V|}\int_{V} \underline{\underline{\sigma}} : \dot{\underline{\underline{\varepsilon}}}\, \mathrm{d}V. \tag{3}$$

Equation (3) has to be modified if discontinuity surfaces exist in the cell for the microscopic velocity field. Note that, for heterogeneous media other than periodic, eqn (3) applies only under particular boundary conditions in terms of stresses or displacements (see e.g. Nemat-Nasser and Hori, 1993). For periodic media, eqn (3) shows that $\underline{\underline{\Sigma}}$ and $\underline{\underline{\dot{E}}}$ are conjugate variables in the expression of the rate-of-work referred to any unit cell. Equation (3) is the basis of energy approaches to evaluate bounds to the yield strength of fiber composites (Suquet, 1982; de Buhan and Taliercio, 1991).

The incremental macroscopic (or homogenized) constitutive law of any composite with periodic structure can be obtained, for instance, by imposing a given macroscopic stress increment to the unit cell and finding the corresponding macroscopic strain rate. This amounts at solving the following problem for the unit cell:

given $\underline{\underline{\dot{\Sigma}}}$, find $\underline{\dot{u}}$ ($\Rightarrow \underline{\underline{\dot{E}}}$) such that

$$\underline{\underline{\dot{\Sigma}}} = \frac{1}{|V|}\int_{\partial V} \underline{x} \otimes (\underline{\dot{\sigma}} \cdot \underline{n})\, \mathrm{d}S \tag{4a}$$

$$\operatorname{div} \underline{\underline{\dot{\sigma}}} = \underline{0} \text{ in } V \tag{4b}$$

$$\underline{\dot{t}} = \underline{\underline{\dot{\sigma}}} \cdot \underline{n} \text{ anti-periodic on } \partial V \tag{4c}$$

$$\underline{\underline{\dot{E}}} = \frac{1}{|V|}\int_{\partial V} \frac{1}{2}(\underline{\dot{u}} \otimes \underline{n} + \underline{n} \otimes \underline{\dot{u}})\, \mathrm{d}S \tag{4d}$$

$$\underline{\dot{u}} - \underline{\underline{\dot{E}}} \cdot \underline{x} \text{ periodic on } V \tag{4e}$$

$$\underline{\underline{\dot{\sigma}}} = f(\underline{\underline{\dot{\varepsilon}}}(\underline{\dot{u}})) \text{ in } V. \tag{4f}$$

In eqns (4a–f) the explicit dependence on $\underline{x}$ of the microscopic variables was dropped for sake of brevity. Equation (4f) represents the microscopic constitutive law at any point of the unit cell, $\underline{\underline{\dot{\varepsilon}}}$ being the strain rate consistent with the displacement rate $\underline{\dot{u}}$. The problem (4a–f) is well posed, for instance, in the linear elastic case (Suquet, 1982): in this case, a formulation in terms of total variables is obviously possible instead of an incremental one. The well-posedness of problem (4a–f) was also shown by Suquet (1982) for dissipative standard components, such as elastoplastic, strain–hardening components following the normality rule.

The homogenization problem (4a–f) has been applied by other authors, either in incremental or finite form, to periodic media other than FRCs. Marigo et al. (1987) employed this approach to describe the macroscopic response of elasto-plastic, regularly perforated plates. More recently, Anthoine (1995) applied the same formulation to derive the in-plane elastic characteristics of brick masonry. In both cases, comparisons with available experimental results and the theoretical predictions of other authors confirmed the reliability of the proposed approach.

3. Numerical model

3.1. Finite element discretization

In this paper, only the response of FRCs subjected to loads acting in any plane transverse to the fibers is investigated. Thus, a two-dimensional (2-D) finite element discretization of a unit cell

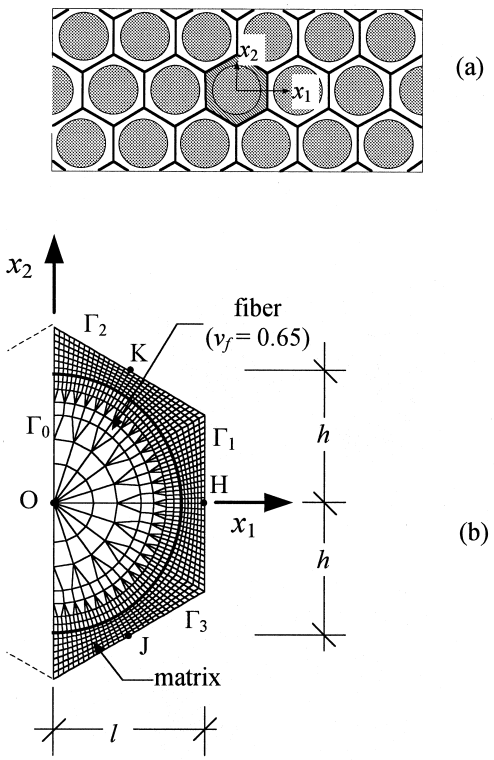

Fig. 3. (a) Hexagonal reinforcing array and unit cell; (b) geometry of the unit cell and finite element discretization.

lying in any plane transverse to the fibers is performed. To make the 2-D model representative of a long-fiber composite subjected to transverse loads, numerical analyses would have to be carried out assuming 'generalized' plane strain conditions (see, e.g., the work by Francescato and Pastor, 1997). In the present work, the fibers are much stiffer than the matrix and prevent the composite to deform in the axial direction. Thus, strains can be reasonably supposed to be locally plane and all analyses are carried out assuming plane strain conditions for the sake of simplicity.

Considering a regular hexagonal reinforcing array, a possible choice for the unit cell is shown in Fig. 3(a). Both x_1 and x_2 are symmetry axes for the cell. Provided that suitable boundary conditions are imposed along one of the symmetry axis, only one half of the cell can be analyzed. Since the stress gradient is likely to be higher in the matrix than in the fiber, a finer discretization was performed in the matrix region. The selected hexagonal cell naturally lends itself to be evenly subdivided into finite elements with aspect ratio near to one. Also, the finite elements have no prevailing orientation. These features are important, since, when BMCs are dealt with, mesh-orientation effects might significantly affect the finite element solution in terms of crack orientation and macroscopic response.

The finite element mesh adopted in applications is shown in Fig. 3(b): it consists of 630 four-noded elements in the entire matrix region and of 350 three- and four-noded elements in the fiber region. The total number of nodes, each having two degrees of freedom, is 1114. This mesh was selected based on a mesh-sensitivity study presented in Section 4.2.1.

The kinematic boundary conditions to be imposed over the boundary of the half-cell in any analyses are explicitly derived in the Appendix and are reported here for sake of clarity. Referring to Fig. 3(b), these conditions read:

$$\underline{u}(O) = \underline{0} \tag{5a}$$

$$\frac{2 \cdot u_{1,\mathrm{K}} - u_{1,\mathrm{H}}}{2h} - \frac{u_{2,\mathrm{H}}}{l} = 0 \tag{5b}$$

$$\underline{u}(\underline{x}_{\mathrm{A}}) + \underline{u}(\underline{x}_{\mathrm{B}}) = 2 \cdot \underline{u}(\underline{x}_{\mathrm{C}}) \quad \forall A, B \in \Gamma_i : \tfrac{1}{2}(\underline{x}_{\mathrm{A}} + \underline{x}_{\mathrm{B}}) = \underline{x}_{\mathrm{C}} \tag{5c}$$

$$\underline{u}(\underline{x}_{\mathrm{H}}) = \underline{u}(\underline{x}_{\mathrm{K}}) + \underline{u}(\underline{x}_{\mathrm{J}}). \tag{5d}$$

Here Γ_i ($i = 0, 1, 2, 3$) is any side of the half-cell, C is the mid-point of Γ_i (i.e. C = O, H, K or J), A and B are any pair of points on Γ_i symmetric with respect to C. Equations (5a, b) suppress any rigid-body motion of the cell, whereas eqns (5b, c) ensure strain-periodicity and compatibility of the displacement field across adjacent cells.

3.2. Simulation of elementary macroscopic strains and stresses

To simulate the composite behaviour under increasing elementary strains, the unit cell has to be analyzed with suitable boundary conditions. As shown in the Appendix, these conditions involve only two points on the cell boundary (H and K in Fig. 3(b), for instance) and can be obtained from eqn (A5). Macroscopic uniaxial strains along x_1 and x_2 (E_{11}, E_{22}) can be obtained, respectively, by imposing:

$$\begin{cases} u_{1,\mathrm{H}} = E_{11} \cdot l \\ u_{2,\mathrm{H}} = 0 \\ u_{2,\mathrm{K}} = 0 \end{cases} \Rightarrow \underline{\underline{E}} = \begin{bmatrix} E_{11} & 0 \\ 0 & 0 \end{bmatrix} \tag{6a}$$

$$\begin{cases} u_{1,\mathrm{H}} = 0 \\ u_{2,\mathrm{H}} = 0 \\ u_{2,\mathrm{K}} = E_{22} \cdot h \end{cases} \Rightarrow \underline{\underline{E}} = \begin{bmatrix} 0 & 0 \\ 0 & E_{22} \end{bmatrix} \tag{6b}$$

and a pure macroscopic shear strain (E_{12}) can be simulated by imposing

$$\begin{cases} u_{1,\mathrm{H}} = 0 \\ u_{2,\mathrm{H}} = E_{12} \cdot l \\ u_{2,\mathrm{K}} = \dfrac{1}{2} \cdot u_{2,\mathrm{H}} = E_{12} \cdot \dfrac{l}{2} \end{cases} \Rightarrow \underline{\underline{E}} = \begin{bmatrix} 0 & E_{12} \\ E_{12} & 0 \end{bmatrix}. \tag{6c}$$

Equations (5), in conjunction with any combination of eqns (6a, b, c), form the complete set of displacement boundary conditions to be imposed on the cell perimeter to reproduce any macroscopic strain.

The simulation of prescribed macroscopic stress conditions in a displacement-based approach is more complicated. An iterative procedure has in general to be used to modify the boundary

displacement increments, at any step of the nonlinear analysis, to simulate prescribed macroscopic stress increments. In the present work, attention is limited to elementary macroscopic stress conditions, namely uniaxial tension along x_1 or x_2 (Σ_{11} and Σ_{22}) and pure shear Σ_{12}. In these cases, symmetry considerations allow reproducing any elementary macroscopic stress by simply imposing displacement boundary conditions at points H and K according to the following scheme:

$$u_{1,\mathrm{H}} \neq 0 \Rightarrow \underline{\underline{\Sigma}} = \begin{bmatrix} \Sigma_{11} & 0 \\ 0 & 0 \end{bmatrix}; \tag{7a}$$

$$\begin{matrix} u_{2,\mathrm{K}} \neq 0 \\ u_{2,\mathrm{H}} = 0 \end{matrix} \Rightarrow \underline{\underline{\Sigma}} = \begin{bmatrix} 0 & 0 \\ 0 & \Sigma_{22} \end{bmatrix}; \tag{7b}$$

$$u_{2,\mathrm{H}} \neq 0 \Rightarrow \underline{\underline{\Sigma}} = \begin{bmatrix} 0 & \Sigma_{12} \\ \Sigma_{12} & 0 \end{bmatrix}. \tag{7c}$$

3.3. Constitutive model for the components

Since the transverse behaviour of FRCs is investigated, the possibility of fiber failure is disregarded. Fibers are supposed to be elastic, with a linear response throughout the loading history. Perfect bonding at the interface between fiber and matrix is also assumed. Allowing for the possibility of decohesion or slipping between the two phases requires having detailed information regarding the exact nature of the constituents, possible interfacial treatments, formation of an interphase region, etc. (see e.g. Ishida and Koenig, 1986). Since the present work aims at deriving results qualitatively applicable to different BMCs, rather than to a specific type of composite, the possibility of failure at the fiber–matrix interface is not considered. Note, however, that the homogenization approach employed in the present work allows in principle for this possibility (see the theoretical results obtained by Taliercio and Sagramoso (1995) for composites with imperfect interfacial bonding).

In the present study, the brittle behaviour of the matrix was described through the 'concrete' model implemented in the computer program employed for the numerical analyses (ABAQUS version 5.4). This model was originally conceived for plain concrete submitted to multiaxial stresses with moderate confining pressure. When the stress state is essentially compressive, the material response is modeled by an elastic-plastic theory, using Drucker–Prager yield criterion. This portion of the failure locus is denoted as 'compression yield surface' and is shown in Fig. 4(a) for the biaxial case. Associated flow rule and isotropic hardening are then used. The equation of the compression yield surface can be written as

$$f_{\mathrm{c}} = J_2 + \alpha I_1 - k = 0, \tag{8}$$

where I_1, J_2 are the first stress invariant and the second invariant of the deviatoric stress, respectively. α is a nondimensional parameter defined as

$$\alpha = \frac{1}{\sqrt{3}} \frac{\sigma_{\mathrm{bc}} - \sigma_{\mathrm{c}}}{2\sigma_{\mathrm{bc}} - \sigma_{\mathrm{c}}} \tag{9}$$

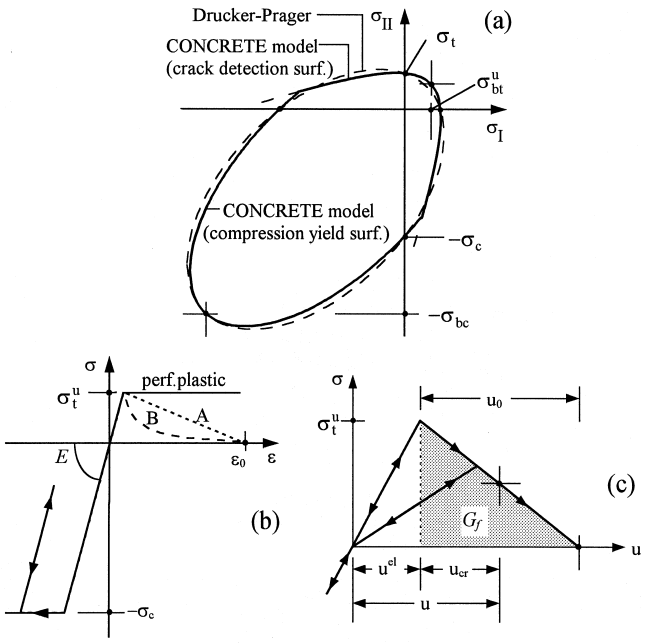

Fig. 4. Assumed behaviour for the matrix material according to ABAQUS 'concrete' model: (a) biaxial failure envelope; (b) uniaxial stress–strain curves; (c) stress–displacement curve in tension for the A-type matrix.

where σ_c = the yield strength of the material in uniaxial compression and σ_{bc} = the yield strength in equi-biaxial compression (see Fig. 4(a)). Finally,

$$k = \left(\frac{1}{\sqrt{3}} - \alpha\right)\sigma_c; \tag{10}$$

$k = k(\lambda_c)$ if the material hardens in compression, where λ_c is a hardening parameter. k is the yield strength in simple shear if the material complies with Drucker–Prager criterion both in tension and compression.

The feature that renders the 'concrete' model particularly suitable for the purposes of this work is the possibility of describing cracking, and the relevant loss in strength and stiffness, by means of a post-peak strain–softening behaviour in tension. Cracking is assumed to occur when the stress point reaches a 'crack detection surface'. The crack detection surface is the Mohr–Coulomb surface (see Fig. 4(a))

$$f_t = \hat{J}_2 + \frac{1}{\sqrt{3}}\left(1 - \beta\frac{\sigma_t(\lambda_t)}{\sigma_t^u}\right)\hat{I}_1 - \frac{1}{\sqrt{3}}\left(2 - \beta\frac{\sigma_t(\lambda_t)}{\sigma_t^u}\right)\sigma_t(\lambda_t) = 0 \tag{11}$$

where the stress measures $\hat{I}_1, \hat{J}_2$ are computed similarly to I_1, J_2, but all stress components associated with 'open cracks' (see below) are neglected in these measures. σ_t^u is the failure stress in uniaxial tension. The nondimensional parameter β is given by

$$\beta = \frac{3\sigma_{bt}^{u} - 2\sigma_{t}^{u}}{2\sigma_{bt}^{u} - \sigma_{t}^{u}} \tag{12}$$

where σ_{bt}^{u} is the failure stress in equi-biaxial tension (see Fig. 4(a)). The relationship $\sigma_t = \sigma_t(\lambda_t)$ defines the post-peak strain–softening behaviour of the material in uniaxial tension, λ_t being an inelastic strain measure ($\sigma_t(0) = \sigma_t^u$).

Both λ_c and λ_t are computed by integration of the multipliers $\dot{\lambda}_c$, $\dot{\lambda}_t$ that define the plastic strain rates, $\dot{\underline{\underline{\varepsilon}}}_c^{pl}$, $\dot{\underline{\underline{\varepsilon}}}_t^{pl}$, associated with the compression yield surface and the crack detection surface, respectively, through associated flow rules:

$$\dot{\underline{\underline{\varepsilon}}}_c^{pl} = \dot{\lambda}_c \frac{\partial f_c}{\partial \underline{\underline{\sigma}}}, \quad \dot{\underline{\underline{\varepsilon}}}_t^{pl} = \dot{\lambda}_t \frac{\partial f_t}{\partial \underline{\underline{\sigma}}}. \tag{13}$$

As soon as a stress point activates the crack detection surface, a 'crack' is supposed to open perpendicularly to the maximum principal component of the corresponding plastic strain rate tensor $\dot{\underline{\underline{\varepsilon}}}_t^{pl}$. The crack orientation $\underline{n}_\alpha$ is kept fixed in the rest of the calculation. Once a crack has formed, a damaged elastic stress–strain law $\underline{\underline{\sigma}} = \underline{\underline{\underline{\underline{D}}}} : \underline{\underline{\varepsilon}}^{el}$, with $\underline{\underline{\varepsilon}}^{el} = \underline{\underline{\varepsilon}} - \underline{\underline{\varepsilon}}_c^{pl}$, is introduced to model the cracked material region. The stiffness component ($D_{\alpha\alpha\alpha\alpha}$) relating the direct stress ($\sigma_{\alpha\alpha}$) and the direct elastic strain ($\varepsilon_{\alpha\alpha}^{el}$) along $\underline{n}_\alpha$ decreases according to a prescribed law (see ABAQUS Theory Manual (1994) for further details). Poisson effects are neglected for open cracks: thus $D_{\alpha\alpha\beta\gamma} = 0$ for $\beta, \gamma \neq \alpha$. In this work, the shear response is supposed to be unaffected by cracking and the elastic shear terms ($D_{\alpha\beta\alpha\beta}$, with $\alpha \neq \beta$) keep their initial undamaged values. Upon unloading, no permanent strain is supposed to be stored in the cracked material along $\underline{n}_\alpha$. Note that 'crack detection' plastic strains, $\underline{\underline{\varepsilon}}_t^{pl}$, are just the outcome of a numerical device to treat cracking: these strains are recast as elastic strains in the direction of cracking and as plastic strains in the other directions.

The ABAQUS concrete model is deemed to be appropriate not only to describe the behaviour of brittle matrix materials, such as ceramics, but also for certain types of polymeric matrices. Indeed, manufacturing processes can induce defects in polymers that originate a brittle behaviour in tension with premature failure (Hull, 1981). Also, thermoplastic resins exhibit different failure modes according to the stress regime (see, e.g., Kinloch and Young, 1983). Under compressive stresses, 'shear yielding' occurs: this type of nonlinear behaviour is essentially plastic, either hardening or perfectly plastic. If the hydrostatic stress is positive, the phenomenon of 'crazing' occurs and the relevant failure mode is brittle. The 'concrete' model employed here reasonably reproduces the Sternstein–Ongchin two-mode failure envelope for polymethyl–methacrylate (Sternstein, 1977) in the stress space, except for the regions where the principal stresses are different in sign.

In the present work, the nonlinear matrix behaviour is described by the uniaxial curves shown in Fig. 4(b). For BMCs, two post-peak curves in tension are considered: one describes a 'smooth' softening behaviour (curve A), that is intended to simulate the progressive degradation of a polymer that entirely loses its bearing capacity only at elevated strains; the other one (curve B) describes a 'sharp' post-peak drop in strength and is rather intended to approach the behaviour of a perfectly brittle matrix material. The perfectly plastic case is also shown in Fig. 4(b).

It must be noted that ABAQUS concrete model is a 'smeared crack model', since it does not

Table 1
Properties of the constituents of the composites considered to validate the model in the elastic field

Glass/epoxy			Modmor/epoxy		
Property	Fiber	Matrix	Property	Fiber	Matrix
E (MPa)	68,940	3420	E_A (MPa)	232,000	5350
v	0.2	0.34	v_A	0.279	0.354
			E_T (MPa)	15,000	5350
			v_T	0.490	0.354
			G_A (MPa)	24,000	1975

describe single cracks, but rather associates to any integration point a region with degraded mechanical properties. Structural analyses involving strain–softening materials are known to be prone to mesh-sensitivity problems: the finite element results do not converge to a unique solution, since a mesh refinement leads to narrower crack bands (see e.g. Crisfield, 1986 for a discussion about this point). In this work, an attempt was made to alleviate mesh-sensitivity by taking the fracture energy, G_f, as a material property (see Section 4.2.1). This requires prescribing the constitutive law for the cracked material by a relationship between stress and 'crack' displacement, $u_{cr} = u - u^{el}$, where u^{el} is the elastic part of the displacement. Crack detection inelastic strains are converted into crack displacements by a 'characteristic length' depending on the mesh size. The uniaxial response of the damaged material is shown in Fig. 4(c) in the case of an A-type matrix submitted to an unloading-reloading cycle.

ABAQUS is capable of performing nonlinear equilibrium analyses involving unstable materials by means of the 'modified Riks method' (see e.g. ABAQUS Theory Manual, 1994); in principle, this method makes it possible to follow also load–displacement curves characterized by a snap-back behaviour (Crisfield, 1986).

4. Analysis of a unit cell subjected to elementary stresses

4.1. Model validation in the elastic field

The reliability of the adopted numerical model was first checked in the linear elastic field by applying it to two composites for which some theoretical and experimental data obtained by other authors were available in the literature (Aboudi, 1991). The considered composites are a glass–epoxy system, with isotropic constituents, and a carbon (Modmor)–epoxy system, with transversely isotropic fibers. The elastic constants of the constituents are listed in Table 1; for Modmor fibers, subscript A refers to the axial direction and subscript T to the transverse direction.

In Fig. 5 the macroscopic transverse elastic modulus and Poisson's ratio of the two composites are plotted vs the fiber volume fraction, v_f. The data plotted in Fig. 5 include the numerical results given by the present model, the results of some experimental tests and the numerical and theoretical

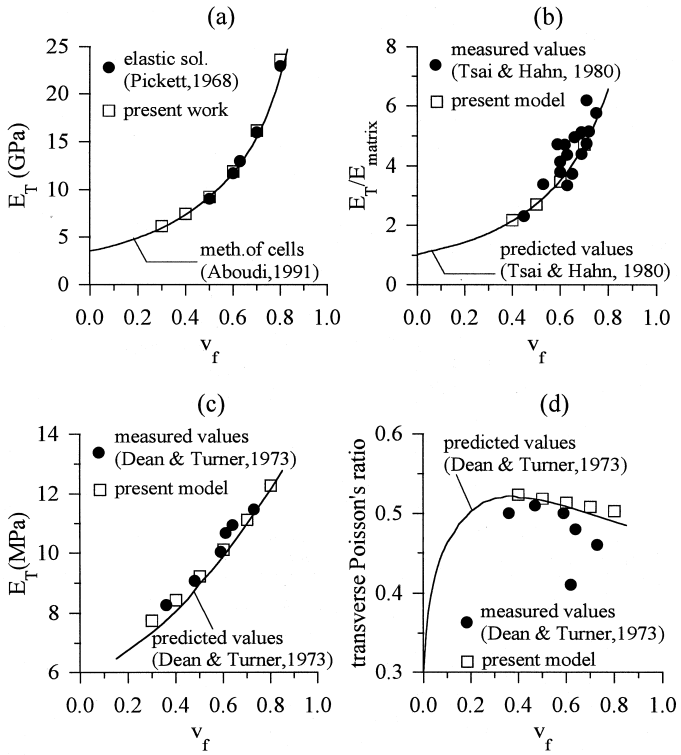

Fig. 5. Elastic properties of two composite materials predicted by the present model and compared with the theoretical and experimental data by other authors (reported in Aboudi, 1991). (a, b): glass–epoxy; (c, d): Modmor–epoxy.

predictions of other researchers, quoted in the captions of Fig. 5. The agreement between model predictions and the other presented results is definitely encouraging.

4.2. Numerical analyses of BMCs subject to elementary stresses

The results of some numerical analyses of composites with non-linear matrix will be now described. First, the mesh reported in Fig. 3(b) and described in Section 3.1 is shown to provide reliable results, as far as the macroscopic strength is concerned, by numerically analyzing the mesh-sensitivity of the results (Section 4.2.1). Then, the cases of uniaxial tension along two different directions in any plane perpendicular to the fibers (Sections 4.2.2 and 4.2.3) and pure transverse shear (Section 4.2.4) are considered.

The elastic and strength properties of the components considered in applications are listed in Table 2. These properties fall within the range of values that can be encountered for E-glass/epoxy composites, with filled matrix that prematurely fractures in tension (see e.g. Hull (1981) and the ASM Engineered Material Handbook—vol. 1, 1987). Note, however, that the aim of this work is to investigate the effects of the matrix brittleness upon the overall composite behaviour, rather than to study a specific material; thus, the selected values are essentially qualitative. The assumed volume fraction, v_f, is 0.65.

Table 2
Properties of the component materials assumed in the nonlinear analyses

	Matrix	Fiber
Young's modulus, E (MPa)	7500	72,000
Poisson's ratio, ν	0.31	0.22
tensile strength, σ_t^u (MPa)	40	—
compressive strength, σ_c (MPa)	140	—
equibiaxial tensile strength, σ_{bt}^u (MPa)	30	—
equibiaxial compressive strength, σ_{bc} (MPa)	224	—

The two post-peak responses in tension corresponding to the uniaxial stress-strain curves A and B in Fig. 4(b) are considered for the matrix. For sake of comparison, the case of a perfectly plastic matrix with the same uniaxial tensile and compressive strength as the brittle one is also analyzed: in this case, the matrix yield surface is defined by the Drucker–Prager's criterion (see Fig. 4(a)). The results of the analyses with perfectly plastic matrix were presented elsewhere (Taliercio, 1997).

The numerical results are presented in terms of macroscopic stress-strain curves and 'crack' distributions. The elements where the matrix softens in tension are shown: cracks are schematized by segments perpendicular to the 'crack' direction $\underline{n}_\alpha$ at any point (see Section 3.3).

4.2.1. Influence of the mesh size on the macroscopic strength

A numerical study was first performed to check the sensitivity of the predicted macroscopic response of the considered BMC to mesh refinement. Three discretizations for the half-cell were considered, namely a 'coarse', a 'medium' and a 'fine' mesh. The coarse and fine meshes are shown in Fig. 6(a) and (b), respectively; the medium mesh was described in Section 3.1 (Fig. 3(b)) and employed in the elastic analyses of Section 4.1. The medium and fine meshes have approximately twice the number of nodes than the relevant coarser mesh in the matrix region.

The three meshes were employed to simulate macroscopic uniaxial tension tests along x_1. In these applications, the post-peak strength of the matrix is supposed to decrease linearly with increasing deformation (A-type matrix). To alleviate the sensitivity of the solution to mesh refinement, in all analyses the postcracking behaviour of the matrix is defined by the same value of the post-peak displacement, u_0, at which the material entirely loses its strength (Fig. 4(c)). In this way, the fracture energy of the material, G_f, is the same regardless of the mesh size. Note that, accordingly, the post-peak stress-strain curve is different in each analysis, since strains and displacements, at any integration point, are related by a characteristic length that depends on the finite element size.

Figure 7 shows the macroscopic stress-strain curves obtained with the three meshes. The medium and fine meshes predict the same macroscopic peak stress and the global post-peak behaviour of the composite, whereas the coarse mesh overpredicts the macroscopic strength and gives a stiffer post-peak response. Thus, no improvement seems to come from the use of a mesh finer than the 'medium' one: this is the mesh used in subsequent applications.

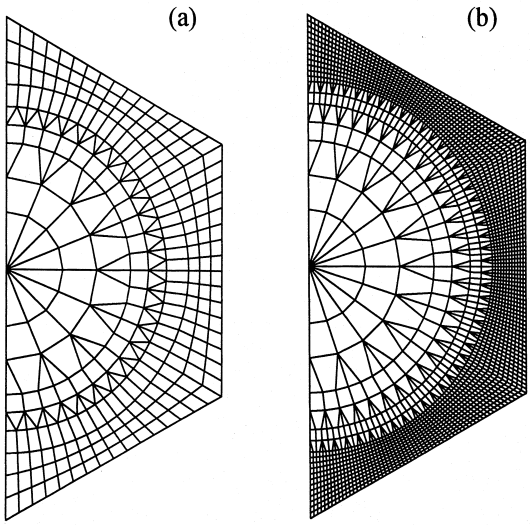

Fig. 6. Mesh-sensitivity analysis: (a) 'coarse'; and (b) 'fine' meshes employed in conjunction with the 'medium' mesh of Fig. 3(b).

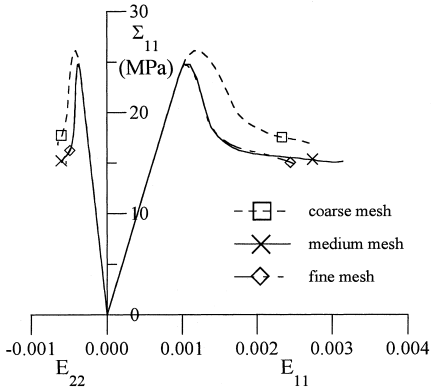

Fig. 7. Mesh-sensitivity analysis: influence of the mesh size on the macroscopic response of an A-type matrix composite subjected to uniaxial tension along x_1 (Σ_{11}).

4.2.2. *Uniaxial tension along* x_1 (Σ_{11})

During the initial elastic stage, the presence of a stiff inclusion (the fiber) 'disturbs' the matrix and induces, on a microscopic level, a stress peak in the matrix region between two adjacent fibers aligned with the applied stress (Fig. 8(a)); in particular, the maximum value of the microscopic stress component σ_{11} exceeds of about 60% the applied macroscopic stress Σ_{11}. If the matrix is brittle, beyond the elastic range damage and inelastic strains progressively localize in that region (Fig. 8(b)). The crack configuration at elevated macroscopic strains is shown in Fig. 8(c): a sort

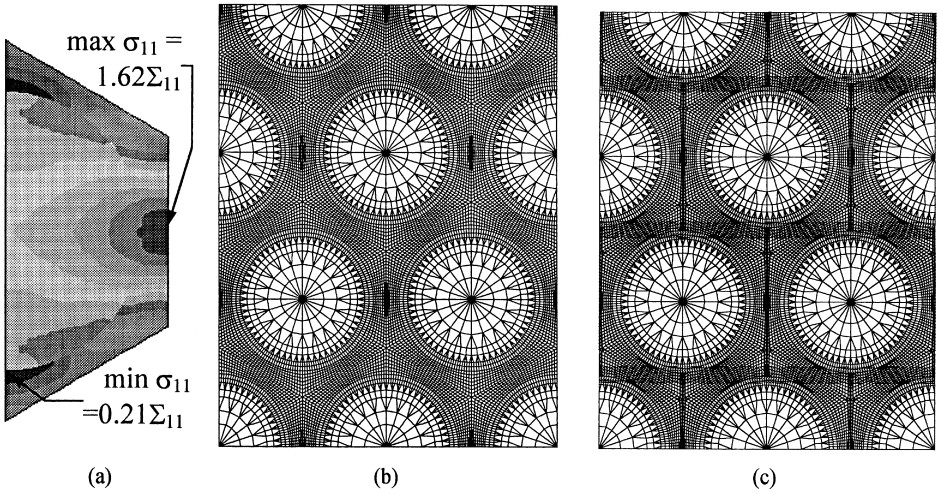

Fig. 8. A-type matrix composite subjected to uniaxial tension along x_1 (Σ_{11}): (a) microscopic stress component σ_{11} in the elastic field; (b) crack pattern in the matrix at the peak stress; (c) final crack pattern: the moderately strained bands that allow stress transmission at elevated macroscopic strains are outlined.

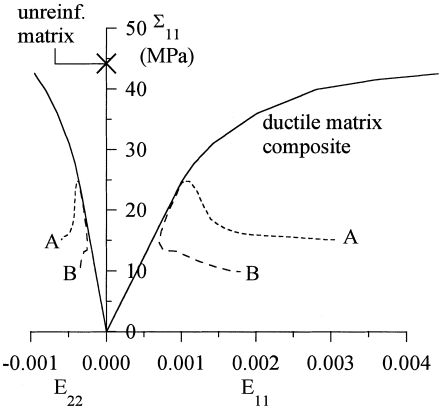

Fig. 9. Macroscopic stress–strain curves for composites with ductile and brittle matrices subjected to macroscopic transverse tension Σ_{11}.

of 'macrocrack' that bridges any pair of adjacent fibers along the axis perpendicular to the applied stress can be identified; another 'macrocrack' tends to develop at the fiber–matrix interface.

The results shown in Fig. 8 refer to a composite with A-type matrix. The evolution of the crack pattern, however, is essentially the same for both A-type and B-type matrix composites. Accordingly, the two types of composites have nearly the same macroscopic strength. This is shown in Fig. 9, where the macroscopic stress–strain curves for the two BMCs subjected to uniaxial transverse tension Σ_{11} are reported and compared with the homologous curve for a ductile–matrix composite. The macroscopic strength of the two BMCs is about one half of the macroscopic yield strength obtained for a perfectly-plastic matrix; it is also much lower than the strength of the

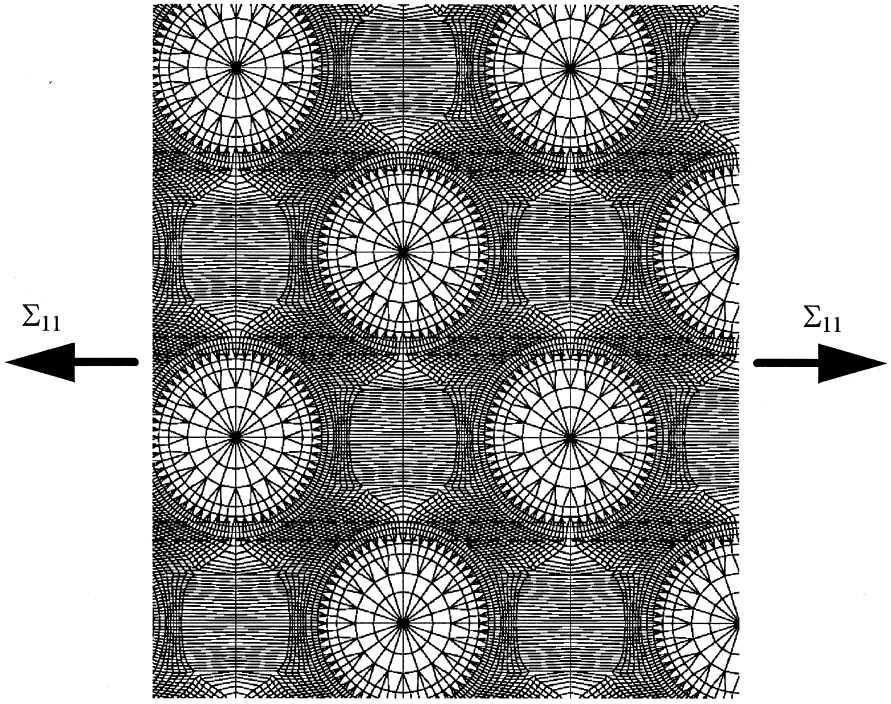

Fig. 10. Deformed assemblage of cells subjected to macroscopic transverse tension Σ_{11}; the moderately strained bands that allow stress transmission at elevated macroscopic strains are outlined.

unreinforced matrix in plane strain conditions (that is, 44.2 MPa), indicated in Fig. 9. Beyond the peak stress, the propagation of damage leads to a sharp decrease in the macroscopic carrying capacity of the composite and a strain-softening behaviour. The sharper drop in strength associated with the B-type matrix composite reflects into a macroscopic post-peak behaviour more brittle than with the A-type matrix composite (Fig. 9).

Note that the composite keeps a non-zero residual strength as the macroscopic strain increases, although the microscopic strain vanishes with increasing microscopic strain. This comes both from the assumed perfect bonding at the fiber-matrix interface and from the fiber volume fraction considered in applications. This can be inferred from Fig. 10 where several deformed unit cells are shown at high macroscopic strain. In the matrix region, bands that run nearly parallel to the applied stress exist, where strains are moderate even at elevated macroscopic strains: it is from these bands that the macroscopic residual strength comes. The bands intersect the tips of the 'macrocracks' orthogonal to the applied stress, where strains are limited because of the assumed perfect interfacial bonding (compare Figs 8(c) and 10). If a BMC with smaller fiber volume fraction were analyzed, the bands would cross the 'macrocracks' in the central highly strained zone, thus preventing stress transmission and giving zero macroscopic residual strength. The interfacial macrocracks (see Fig. 8(c)) do not significantly decrease the load carrying capacity of the bands, because, according to ABAQUS concrete model, the softening behaviour affects only the stress component perpendicular to the crack. This remaining load carrying capacity is likely to be

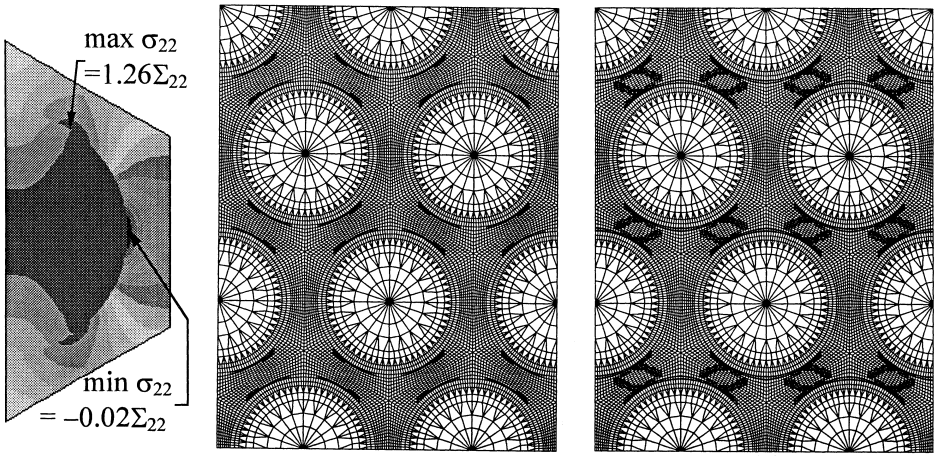

Fig. 11. A-type matrix composite subjected to uniaxial tension along x_2 (Σ_{22}): (a) microscopic stress component σ_{22} in the elastic field; (b) crack pattern in the matrix at the peak stress; (c) final crack pattern.

unrealistic for real BMCs; this inconsistency could be removed by taking an interface criterion into account.

4.2.3. Uniaxial tension along x_2 (Σ_{22})

During the initial elastic stage, on a macroscopic level the composite behaves equally either when stressed along x_1 or along x_2, according to its transversely isotropic nature. The microscopic stress and strain fields corresponding to the two macroscopic stress conditions, however, are different. This can be appreciated comparing Fig. 8(a) and Fig. 11(a): in the latter figure, the distribution of the microscopic stress component σ_{22} associated with a uniaxial macroscopic tension Σ_{22} in the elastic range is shown. Beyond the elastic range, the symmetry in mechanical properties of the material is lost. Damage nucleates at the fiber-matrix interface (Fig. 11(b)) and propagates along this surface until a sort of two-branched macrocrack forms and bridges two adjacent fibers (Fig. 11(c)).

In this case also, the results of the analyses with A-type and B-type matrix are not substantially different as far as the peak stress values and the crack patterns are concerned. This is shown in Fig. 12, where the macroscopic stress-strain curves of the two BMCs and the ductile-matrix composites are reported. The macroscopic strength of the BMC is about 45% lower than the strength of the perfectly plastic composite at (moderately) large strains. The smoother or sharper strain–softening behaviour of the matrix in tension mainly affects the post-peak macroscopic response. The residual strength of the composites can be motivated by arguments similar to those made in the case of uniaxial tension along x_1. The results at elevated macroscopic strains, however, have little interest on account of the many approximations made regarding the behaviour of the phases (see the comment at the end of the previous section).

The different crack patterns in the two cases of uniaxial tension along x_1 or x_2 are matched by an anisotropic behaviour of the composite beyond the elastic field (Fig. 13). In particular, the peak value of the macroscopic stress Σ_{22} exceeds of about 30% the corresponding value in uniaxial

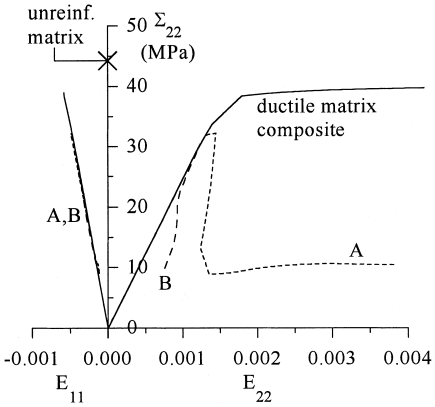

Fig. 12. Macroscopic stress–strain curves for composites with ductile and brittle matrices subjected to macroscopic transverse tension Σ_{22}.

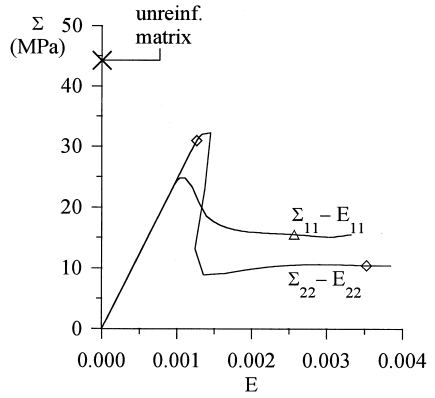

Fig. 13. Comparison of the macroscopic stress–strain curves for composites with A-type matrix subjected to tension along x_1 or x_2.

tension along x_1. Also, the composite behaviour is macroscopically more brittle than in uniaxial tension along x_1. On the contrary, the numerically computed macroscopic yield stresses indicate that the ductile matrix composite maintains its transversely isotropic nature, although its response before failure is different according to the direction of the applied macroscopic stress.

4.2.4. *Pure transverse shear* (Σ_{12})

In the elastic range, the microscopic stress and strain components produced by a macroscopic shear stress Σ_{12} have symmetric (or anti-symmetric) distributions across the cell. Symmetry properties are lost beyond the linear range. This is due to the unsymmetric behaviour of the matrix in tension and compression, rather than to brittleness. The A-type matrix composite starts damaging

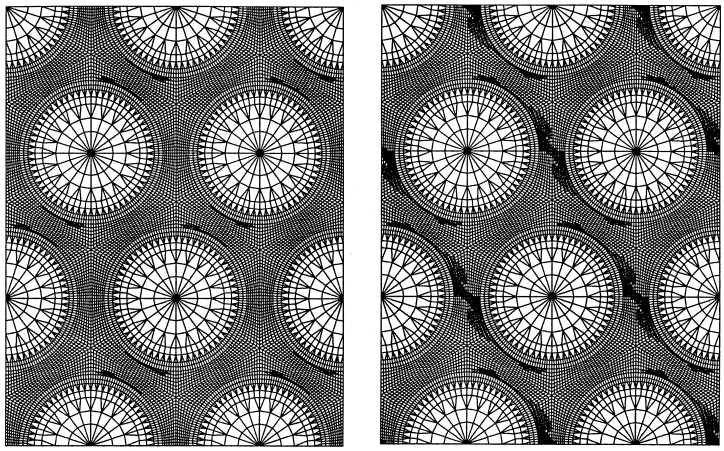

Fig. 14. A-type matrix composite subjected to transverse shear (Σ_{12}): (a) crack pattern in the matrix at the peak stress; (b) final crack pattern.

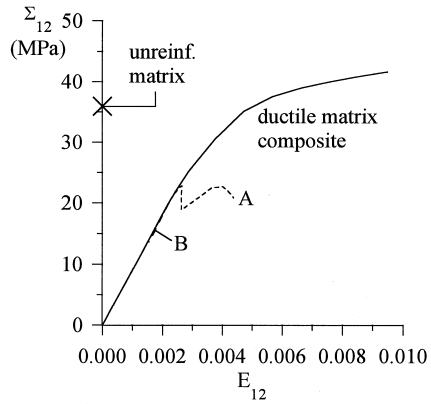

Fig. 15. Macroscopic stress–strain curves for composites with ductile and brittle matrices subjected to macroscopic transverse shear Σ_{12}.

at the interface (Fig. 14(a)). Then cracks propagate so as to bridge two adjacent fibers, and macrocracks form that are essentially perpendicular to the macroscopic principal tensile stress (Fig. 14(b)). Damage nucleation is similar for the B-type matrix composite, but the post-peak drop in strength is so abrupt that the composite response could not be followed. The macroscopic stress–strain curves in pure shear are shown in Fig. 15. Here again, the strength of the BMCs is lower than the pure shear strength of the unreinforced matrix ($k = 35.9$ MPa), indicated in Fig. 15. The ductile matrix composite in pure shear has a progressively strain-hardening behaviour accompanied by an out-of-plane macroscopic compression Σ_{33} beyond the elastic range, so that no macroscopic shear limit could be identified.

5. Discussion and conclusions

A numerical model has been presented to investigate the behaviour of brittle–matrix fiber-reinforced composites subjected to transverse stresses. In principle, the method can be applied to any macroscopic stress conditions—provided that a 3-D finite element model with suitable boundary conditions is developed. The main results of the performed analyses can be summarized as follows:

(a) The macroscopic tensile and shear strengths of a BMC are much lower than both the strength of companion ductile–matrix composites and the strength of the unreinforced matrix. In tension, the predicted macroscopic strength of the considered BMCs is lower of about 45–55% than the strength of a companion ductile matrix composite.
(b) A certain induced anisotropy arises in the damaged BMCs. In any plane transverse to the fibers, the macroscopic tensile strength depends on the direction of the applied stress. The composite exhibits lower tensile macroscopic strength when stressed along x_1, that is, the direction along which the pairs of contiguous fibers have the minimum distance and for which macrocracks form perpendicular to the applied stress.
(c) The slope of the post-peak softening branch does not significantly affect the macroscopic strength, but rather affects the composite post-peak response. This would indicate that the results presented here apply also for ceramic composites with perfectly brittle matrix, as far as the decrease in macroscopic strength is concerned.

In the present work, the use of fracture energy as a material parameter alleviated the mesh sensitivity of the results, as shown by the numerical study illustrated in Section 4.2.1. An alternative approach to the numerical study of BMCs is offered by 'regularization techniques' that involve differential operators of the plastic multipliers and make non-local the constitutive model (see e.g. Comi and Perego, 1996). These techniques can improve the description of the microfields, but are usually computationally expensive. It is believed that the performed analyses can be sufficiently exhaustive to quantify the decrease in strength of a BMC respect to a ductile one, which is the main result of this work.

In the analyses presented in this work, strains were assumed to be small. This may not be the case for polymeric–matrix composites, since some polymers can undergo large strains: this is particularly true beyond the yield point. In present applications, the correctness of this assumption was ascertained 'a posteriori', by checking the smallness of the computed strains.

As a consequence of its theoretical origin, the model presented can only account for the loss in bearing capacity of a composite structure coming from the formation of evenly distributed cracks. This is the situation that would occur in an ideal unbounded medium with exactly periodic mechanical properties. The analysis of any unit cell, assumed to be representative of the entire composite, does not allow one to account for phenomena such as delamination, possibly originated by edge effects, that are often responsible for the failure of laminated structures.

It must also be acknowledged that a more rigorous approach to the homogenization of BMCs would require computations much more complex than those performed here. Indeed, homogenization does not apply in a simple form for periodic media with components possessing a non-convex energy (see, e.g., Müller, 1987). Instead of one cell, all solutions that are periodic over an ensemble of cells, which is not known a priori, have to be considered to compute the exact energy

stored in the homogenized material. This homogenization result is very difficult to use in practice and the dependence of the findings on the number of unit cells has not been investigated in this work. Thus, in principle the approach employed here predicts a homogenized behaviour 'stiffer' than the exact one.

The assumed periodicity in the model might lead to results not appropriate for real composites, reinforced by a random array of fibers. This was numerically shown by Brockenborough et al. (1991) for ductile matrix composites under transverse tension. Note, however, that the same authors also showed that a periodic hexagonal reinforcing array, of the type considered here, allows matching the 'exact' results yielded by a nonperiodic array more closely than other types of periodic fiber packing arrangements.

The presented numerical predictions await now a confirmation by experimental test data, also on account of the many simplifications made and listed above.

Future developments of the present works will aim at taking interface effects into account (see also the discussion in Section 3.3) and at extending the analyses to different types of matrix behaviour. For unidirectional polymeric composites subjected to transverse loads time effects can be extremely significant (see, e.g., Chen et al., 1995), so that creep strains in the matrix cannot be neglected. The approach employed here would be alternative to the semi-analytical method recently proposed by Fotiu and Nemat-Nasser (1996) for viscoplastic composites, or the micromechanical approach based on the use of Eshelby's equivalent-inclusion principle by Chen et al. (1995) for linear viscoelastic composites.

Appendix: Displacement boundary conditions

In this Appendix, the kinematic boundary conditions that were imposed in the numerical analyses of the unit cell to ensure strain-periodicity of the microscopic displacement field will be derived.

Consider the hexagonal unit cell shown in Fig. A1(a) and define an orthonormal reference system (Ox_1x_2) with origin in the center of the cell. The boundary ∂V of the entire cell can be subdivided into several parts: $\partial V = \Gamma_1 \bigcup \Gamma_1' \bigcup \Gamma_2 \bigcup \Gamma_2' \bigcup \Gamma_3 \bigcup \Gamma_3'$; the boundary of the discretized half-cell consists of the parts Γ_1, Γ_2 and Γ_3, in addition to the segment Γ_0 of the symmetry axis x_2.

In all numerical applications, boundary conditions were imposed to suppress any rigid body motions of the cell. The condition

$$\underline{u}(O) = \underline{0} \tag{A1}$$

suppresses rigid translations. To suppress rigid rotations preserving the periodicity requirements of the displacement field, it is first necessary to establish relationships between the macroscopic strains and the components of the microscopic displacements at some points. Let eqn (2) be written for points K and K′ (Fig. A1(a)); if the symmetry condition $\underline{u}(\underline{x}_K) = -\underline{u}(\underline{x}_{K'})$ is imposed, along with the periodicity condition $\underline{v}(\underline{x}_K) = \underline{v}(\underline{x}_{K'})$, one gets

$$2 \cdot \underline{u}(\underline{x}_K) = \underline{\underline{E}} \cdot (\underline{x}_K - \underline{x}_{K'}) \equiv E \cdot \underline{w}_2 \tag{A2}$$

Similarly, considering points H and H′ the condition

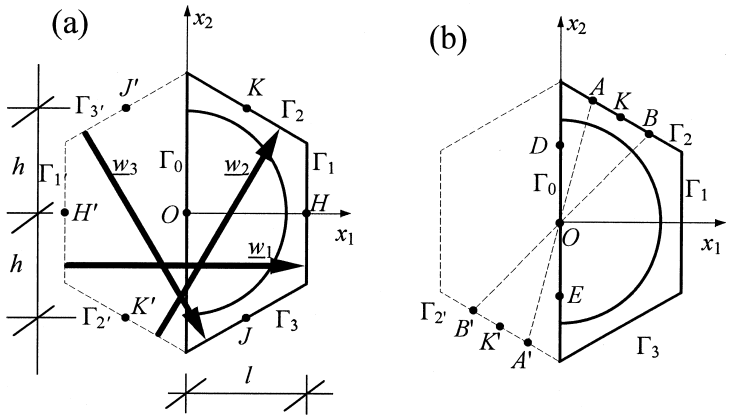

Fig. A1. Description of the discretized unit cell: (a) segments forming the boundary; (b) typical points involved in symmetry and periodicity conditions.

$$2\cdot\underline{u}(\underline{x}_{\mathrm{H}}) = \underline{\underline{E}}\cdot\underline{w}_1 \tag{A3}$$

is obtained. In explicit form, eqns (A2) and (A3) read

$$2\cdot\underline{u}(\underline{x}_{\mathrm{K}}) = \underline{\underline{E}}\cdot\underline{w}_2 \Leftrightarrow \begin{cases} 2\cdot u_{1,\mathrm{K}} = E_{11}\cdot l + E_{12}\cdot 2\cdot h \\ 2\cdot u_{2,\mathrm{K}} = E_{21}\cdot l + E_{22}\cdot 2\cdot h \end{cases}; \tag{A4a}$$

$$2\cdot\underline{u}(\underline{x}_{\mathrm{H}}) = \underline{\underline{E}}\cdot\underline{w}_1 \Leftrightarrow \begin{cases} 2\cdot u_{1,\mathrm{H}} = E_{11}\cdot 2\cdot l \\ 2\cdot u_{2,\mathrm{H}} = E_{21}\cdot 2\cdot l \end{cases} \tag{A4b}$$

Thus, the components of the macroscopic strain tensor $\underline{\underline{E}}$ can be expressed in terms of the displacement components of H and K:

$$\underline{\underline{E}} = \begin{bmatrix} E_{11} & E_{12} \\ E_{21} & E_{22} \end{bmatrix} = \begin{bmatrix} \dfrac{u_{1,\mathrm{H}}}{l} & \dfrac{2\cdot u_{1,\mathrm{K}} - u_{1,\mathrm{H}}}{2h} \\ \dfrac{u_{2,\mathrm{H}}}{l} & \dfrac{2\cdot u_{2,\mathrm{K}} - u_{2,\mathrm{H}}}{2h} \end{bmatrix} \tag{A5}$$

Imposing the symmetry of tensor $\underline{\underline{E}}$ amounts at suppressing the (infinitesimal) rigid rotations of the cell. The condition $E_{12} = E_{21}$ gives

$$\frac{2\cdot u_{1,\mathrm{K}} - u_{1,\mathrm{H}}}{4h} - \frac{u_{2,\mathrm{H}}}{2l} = 0. \tag{A6}$$

The boundary conditions that reproduce the strain-periodicity requirement for the displacement field and ensure inter-elemental continuity of the deformed cells are now derived. Consider any side of the cell, e.g. Γ_2 (Fig. A1(b)), the mid-point of this side (K, for side Γ_2) and two points (A, B) on the same side symmetric with respect to it. If eqn (2) is specialized to these points, one gets:

$$\underline{u}(\underline{x}_A) = \underline{\underline{E}} \cdot \underline{x}_A + \underline{v}(\underline{x}_A) \tag{A7a}$$

$$\underline{u}(\underline{x}_B) = \underline{\underline{E}} \cdot \underline{x}_B + \underline{v}(\underline{x}_B) \tag{A7b}$$

$$\underline{u}(\underline{x}_K) = \underline{\underline{E}} \cdot \underline{x}_K + \underline{v}(\underline{x}_K) \tag{A7c}$$

Combining eqns (A7a–c) and noting that $\underline{x}_K = \frac{1}{2}(\underline{x}_A + \underline{x}_B)$ yields:

$$\underline{u}(\underline{x}_A) + \underline{u}(\underline{x}_B) - 2 \cdot \underline{u}(\underline{x}_K) = \underline{v}(\underline{x}_A) + \underline{v}(\underline{x}_B) - 2 \cdot \underline{v}(\underline{x}_K). \tag{A8a}$$

Similarly, for the side opposite to Γ_2 (i.e. Γ_2') one has

$$\underline{u}(\underline{x}_{A'}) + \underline{u}(\underline{x}_{B'}) - 2 \cdot \underline{u}(\underline{x}_{K'}) = \underline{v}(\underline{x}_{A'}) + \underline{v}(\underline{x}_{B'}) - 2 \cdot \underline{v}(\underline{x}_{K'}). \tag{A8b}$$

The deformed cell must possess the same central symmetry respect to O as the undeformed one. Thus:

$$\underline{u}(\underline{x}_A) = -\underline{u}(\underline{x}_{A'}); \quad \underline{u}(\underline{x}_B) = -\underline{u}(\underline{x}_{B'}); \quad \underline{u}(\underline{x}_K) = -\underline{u}(\underline{x}_{K'}). \tag{A9}$$

Also, referring to the periodic part of the displacement field:

$$\underline{v}(\underline{x}_A) = \underline{v}(\underline{x}_{B'}); \quad \underline{v}(\underline{x}_B) = \underline{v}(\underline{x}_{A'}); \quad \underline{v}(\underline{x}_K) = \underline{v}(\underline{x}_{K'}) \tag{A10}$$

Substituting eqns (A9), (A10) in eqn (A8b) and combining it with eqn (A8a) yields the condition that relates the displacements of any pair of points A, B on Γ_2, symmetric respect to the mid-point K of this side, to the displacement of K itself:

$$\underline{u}(\underline{x}_A) + \underline{u}(\underline{x}_B) = 2 \cdot \underline{u}(\underline{x}_K) \quad \forall A, B \in \Gamma_2 \quad \text{such that } \tfrac{1}{2}(\underline{x}_A + \underline{x}_B) = \underline{x}_K \tag{A11}$$

Similar conditions obviously apply along Γ_1 and Γ_3. Along the symmetry axis x_2 the periodic part of the displacement field must vanish. Thus, for any pair of points $D, E \in \Gamma_0$, symmetric respect to the center O (i.e. with $\underline{x}_D = -\underline{x}_E$, Fig. A1(b)) the condition

$$\underline{u}(\underline{x}_D) + \underline{u}(\underline{x}_E) = \underline{0} \tag{A12}$$

holds. In addition to the conditions derived up to here, a relationship must be found to ensure that the deformed sides all belong to the boundary of the same deformed half-cell. An equation similar to eqns (6) and (7) can be written for the mid-point of J of side Γ_3 (see Fig. A1(a)):

$$2 \cdot \underline{u}(\underline{x}_J) = \underline{\underline{E}} \cdot \underline{w}_3. \tag{A13}$$

Equations (A2), (A3), (A13) and the condition $\underline{w}_1 = \underline{w}_2 + \underline{w}_3$ lead to the relationship sought, that involves the displacement of the mid-points of the outer boundary of the half-cell:

$$\underline{u}(\underline{x}_H) = \underline{u}(\underline{x}_K) + \underline{u}(\underline{x}_J) \tag{A14}$$

In conclusion, eqns (A4), (A6), (A11) and (A14) form the set of conditions to be imposed over the boundary of the half-cell in any finite element analysis (see also eqns (5a–d) in Section 3.1).

Acknowledgments

This work was developed within the framework of a research supported by MURST, the Italian Ministry for University. The most valuable suggestions of Dr Armelle Anthoine are also gratefully acknowledged.

References

ABAQUS Theory Manual version 5.4, 1994. Hibbit, Karlsson and Sorensen Inc., Pawtucket, RI.

Aboudi, J., 1988. Constitutive equations for elastoplastic composites with imperfect bonding. Int. J. Plasticity 4, 103–125.

Aboudi, J., 1991. Mechanics of composite materials—a unified micromechanical approach. Elsevier, Amsterdam.

Anthoine, A., 1995. Derivation of the in-plane elastic characteristics of masonry through homogenization theory. Int. J. Solids Structures 32, 137–163.

ASM International Handbook Committee, 1987. Engineered Material Handbook—vol. 1: Composites. ASM International, Metals Park, Ohio.

Bosco, C., Carpinteri, A., 1995. Discontinuous constitutive response of brittle matrix fibrous composites. J. Mech. Phys. Solids 43, 261–274.

Brockenborough, J.R., Suresh, S., Wienecke, H.A., 1991. Deformation of metal-matrix composites with continuous fibers: geometrical effects of fiber distribution and shape, Acta Metall. Mater. 39, 735–752.

Chen, C.H., Chang, Y.H., Cheng, C.H., 1995. Micromechanics and creep behaviour of fiber-reinforced PEEK composites. J. Compos. Mater. 29, 359–371.

Comi, C., Perego, U., 1996. A generalized variable formulation for gradient-dependent softening plasticity. Int. J. Numer. Methods Engng 39, 3731–3755.

Crisfield, M.A., 1986. Snap-through and snap-back response in concrete structures and the dangers of under-integration. Int. J. Numer. Methods Engng 22, 751–767.

de Buhan, P., Taliercio, A., 1991. A homogenization approach to the yield strength of composite materials. Eur. J. Mech. A/Solids 10, 129–154.

Dharani, L.R., Ji, F.S., 1996. Non-axisymmetric matrix cracking in unidirectional brittle matrix composites. Engng Fracture Mech. 53, 57–68.

Dvorak, G.J., Bahei-el-Din, Y.A., 1987. A bimodal plasticity theory of fibrous composite materials. Acta Mech. 69, 219–241.

Dvorak, G.J., Bahei-el-Din, Y.A., 1991. Experiments and modelling in plasticity of fibrous composites. In: Dvorak, G. J. (Ed.), Inelastic Deformation of Composite Materials. Springer-Verlag, New York, pp. 283–306.

Dvorak, G.J., Bahei-el-Din, Y.A., Macheret, Y., Liu, C.H., 1988. An experimental study of elastic–plastic behaviour of a fibrous boron-aluminium composite. J. Mech. Phys. Solids 36, 655–687.

Fotiu, P.A., Nemat-Nasser, S., 1996. Overall properties of elastic–viscoplastic periodic composites. Int. J. Plasticity 12, 163–190.

Francescato, P., Pastor, J., 1997. Lower and upper numerical bounds to the off-axis strength of unidirectional fiber-reinforced composites by limit analysis methods. Eur. J. Mech. A/Solids 16, 213–234.

Hashin, Z., 1965. Viscoelastic behaviour of heterogeneous media. J. Appl. Mech., ASME 32, 630–636.

Hashin, Z., 1966. Viscoelastic fiber reinforced materials. AIAA Journal 4, 1411–1417.

Hild, F., Burr, A., Leckie, F.A., 1996. Matrix cracking and debonding of ceramic-matrix composites. Int. J. Solids Structures 33, 1209–1220.

Hull, D., 1981. An Introduction to Composite Materials. University Press, Cambridge, U.K.

Ishida, H., Koenig, J.L., 1986. Composite interfaces. North-Holland, New York.

Kinloch, A.J., Young, R.J., 1983. Fracture Behaviour of Polymers. Appl. Sci. Pub., London.

Marigo, J.J., Mialon, P., Michel, J.C., Suquet, P., 1987. Plasticité et homogénéisation: un example de prévision des charge limites d'une structure hétérogène périodique. J. Méc. Th. Appl. 6, 47–75.

Müller, S., 1987. Homogenization of nonconvex integral functionals and cellular elastic materials. Arch. Rat. Mech. Anal. 99, 189–212.

Nemat-Nasser, S., Hori, M., 1993. Micromechanics: Overall Properties of Heterogeneous Materials, North-Holland, Amsterdam.

Pindera, M.J., Aboudi, J., 1988. Micromechanical analysis of yielding of metal matrix composites. Int. J. Plasticity 4, 195–214.

Sternstein, S.S., 1977. Mechanical properties of glassy polymers. In: Shultz, J.M. (Ed.), Treatise on Material Science and Technology—vol. 10: Properties of solid polymeric materials—Part B, Academic Press, New York.

Suquet, P., 1982. Plasticité et homogénéisation. Ph.D. thesis, Université Paris VI.

Suquet, P., 1987. Elements of homogenization for inelastic solid mechanics. In: E. Sanchez-Palencia, E., Zaoui, A. (Ed.), Homogenization Techniques for Composite Media. Lecture Notes in Physics 272. Springer, New York. pp. 193–278.

Taliercio, A., 1992. Lower and upper bounds to the macroscopic strength domain of a fiber-reinforced composite material. Int. J. Plasticity 8, 741–762.

Taliercio, A., 1997. Homogenization of elastoplastic composites. Proc. ICCE/4, Kona Big Island, Hawaii, pp. 971–972.

Taliercio, A., Sagramoso, P., 1995. Uniaxial strength of polymeric-matrix fibrous composites predicted through a homogenization approach. Int. J. Solids Structures 32, 2095–2123.

Zhang, H.Q., Delale, F., Liaw, B.M., 1996. Interface and matrix fracture in brittle fiber-reinforced composites. Int. J. Solids Structures 33, 249–273.